AGU PUBLICATIONS

Geophysical Research Letters

RESEARCH LETTER
10.1002/2015GL067432

Key Points:
- *F* region field-aligned irregularities (FAIs) at magnetically low latitudes are studied
- Freshly growing of FAIs was observed using two-dimensional map of Equatorial Atmosphere Radar
- The vertical velocities of evolving FAIs are smaller at postmidnight than at postsunset

Correspondence to:
T. Dao,
tamdao@stelab.nagoya-u.ac.jp

Citation:
Dao, T., Y. Otsuka, K. Shiokawa, S. Tulasi Ram, and M. Yamamoto (2016), Altitude development of postmidnight *F* region field-aligned irregularities observed using Equatorial Atmosphere Radar in Indonesia, *Geophys. Res. Lett.*, *43*, doi:10.1002/2015GL067432.

Received 14 DEC 2015
Accepted 19 JAN 2016
Accepted article online 20 JAN 2016

Altitude development of postmidnight *F* region field-aligned irregularities observed using Equatorial Atmosphere Radar in Indonesia

Tam Dao[1,2], Yuichi Otsuka[1], Kazuo Shiokawa[1], S. Tulasi Ram[3], and Mamoru Yamamoto[4]

[1]Institute for Space-Earth Environmental Research, Nagoya University, Nagoya, Japan, [2]Institute of Physics, VAST, Ho Chi Minh City, Vietnam, [3]Indian Institute of Geomagnetism, Navi Mumbai, India, [4]Research Institute for Sustainable Humanosphere, Kyoto University, Uji, Japan

Abstract For the first time, vertical rise velocities of postmidnight field-aligned irregularities (FAIs) at low geomagnetic latitudes have been examined near the June solstice by using two-dimensional maps of *F* region FAI echoes observed with the Equatorial Atmosphere Radar in Indonesia for 3 years starting in May 2010. We found 15 freshly growing FAIs at postmidnight between May and August during the 3 years. The rise velocities of FAIs are smaller at postmidnight than at postsunset, and most postmidnight FAIs do not exceed an altitude of 450 km. Based on the rise velocities, a lower limit for the creation time of the postmidnight FAIs is estimated to be between 21:30 LT and 02:00 LT for 14 of the 15 events, indicating that this class of FAIs is distinct from the postsunset FAIs.

1. Introduction

In the nighttime equatorial and low-latitude ionosphere, plasma density irregularities with a spectrum of spatial scale sizes, ranging from a few centimeters to a few hundred kilometers, are often accompanied by a plasma bubble, which is a localized severe depletion of ionospheric plasma density [*Haerendel*, 1974]. These irregularities have been detected by using various ground-based radio and optical probing techniques in addition to satellite in situ probes. Plasma bubbles are observed as diffused or spread echoes on ionograms, and so they are often called equatorial spread *F* (ESF). Field-aligned irregularities (FAIs) in plasma bubbles growing upward from the bottomside *F* layer were first observed by *Woodman and LaHoz* [1976] with a VHF radar in Jicamarca, Peru. Subsequent studies have extensively investigated the generation, growth, and dynamics of plasma bubbles.

A plasma bubble can be initiated at the bottomside of the *F* region over the magnetic equator when the eastward electric field is enhanced at sunset (so-called prereversal enhancement (PRE)), and it grows through the Rayleigh-Taylor instability [*Kelley*, 2009]. The seasonal variation of the occurrence rate of these plasma bubbles is consistent with that of the eastward electric field, which is enhanced when the sunset terminator is parallel to the geomagnetic field line [*Tsunoda*, 1985]. In the Asian longitudinal sector, where the geomagnetic field line is aligned in the meridional direction, plasma bubbles frequently occur around equinoxes [*Burke et al*., 2004]. The occurrence rate of plasma bubbles increases with solar activity because the eastward electric field increases as well. However, *Otsuka et al*. [2009] reported that FAIs observed with a 30.8 MHz radar at Kototabang, Indonesia, frequently occur at postmidnight around the June solstice during a solar minimum period. A high occurrence rate of postmidnight FAI has also been observed around the June solstice in India [*Patra et al*., 2009] and Brazil [*Candido et al*., 2011], as well as around the December solstice in the central Pacific [*Miller et al*., 2010]. In situ plasma density measurements by the Communication/Navigation Outage Forecasting System (C/NOFS) satellite also showed plasma density irregularities occurring at postmidnight [*Heelis et al*., 2010]. *Yokoyama et al*. [2011] compared the postmidnight FAIs with the plasma density irregularities observed by the C/NOFS in situ measurements. They suggested that the postmidnight irregularities could be associated with either plasma bubbles or medium-scale traveling ionospheric disturbances (MSTIDs), which frequently appeared at midlatitudes and propagated equatorward and westward.

Using multiple beam measurements of *F* region FAIs with the Equatorial Atmosphere Radar (EAR) at Kototabang, Indonesia, *Yokoyama et al*. [2004] revealed that the onset of FAIs during high solar activity conditions mainly occurred at sunset at the altitude of the apex of the geomagnetic field line connected with the

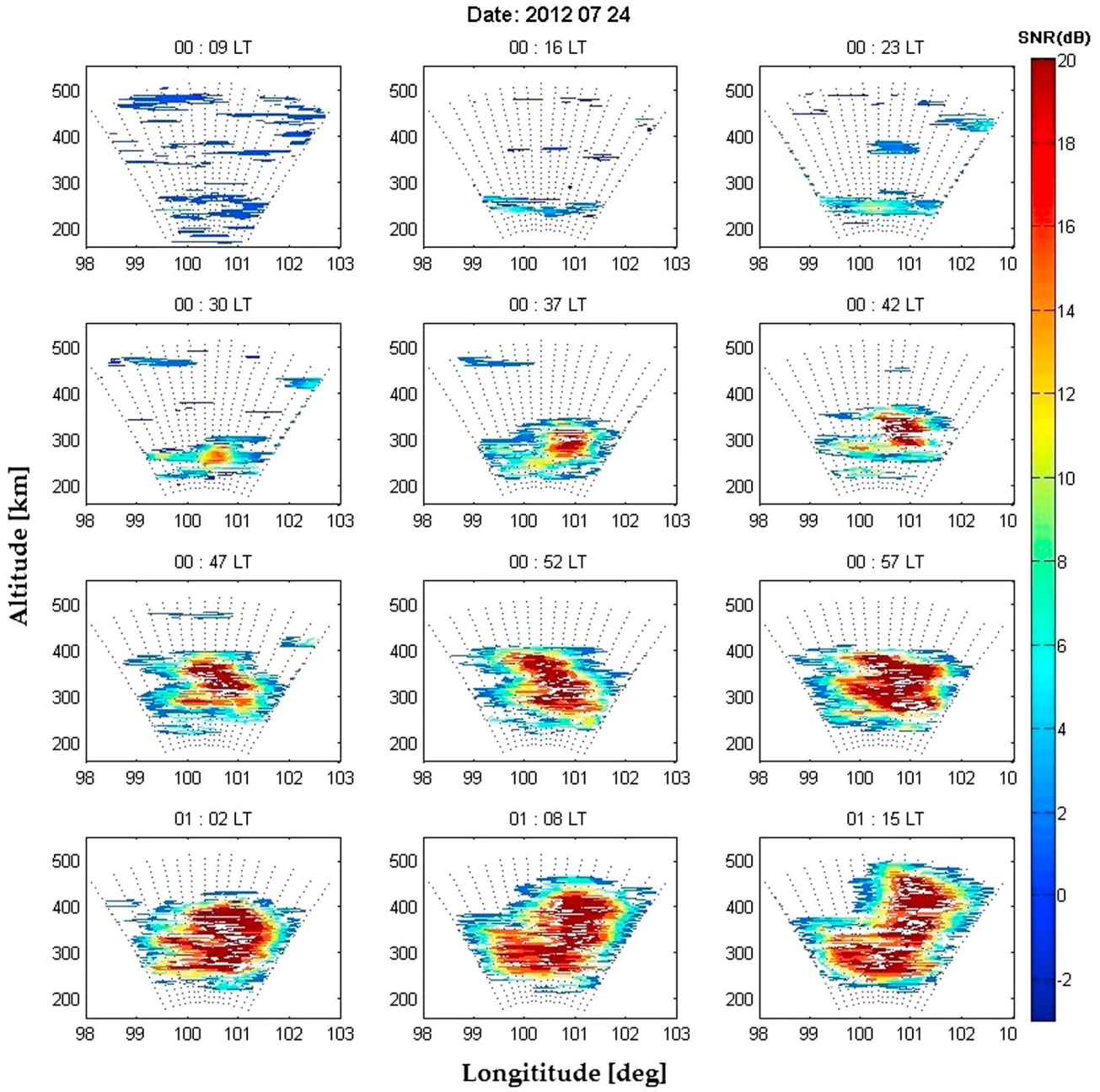

Figure 1. Time sequence of two-dimensional maps of the *F* region FAI echo intensity observed with the EAR between 00:09 and 01:15 LT on 24 July 2012.

observed area. *Yokoyama and Fukao* [2006] investigated the rise velocity of the FAI region at postsunset and noted that the observed rise velocity is consistent with the nonlinear evolution of plasma bubbles as simulated by previous numerical studies. With regard to postmidnight FAIs, *Ajith et al*. [2015] showed that FAIs appearing around midnight grow to higher altitudes in the field of view (FOV) of the EAR. However, the rise velocities of postmidnight FAIs have not been studied systematically.

In this study, we have investigated the rise velocity of *F* region FAI echoes observed with the EAR for 3 years, from May 2010 to June 2013. We found a clear difference between the rise velocities of the postsunset and the postmidnight FAIs. Using these observational results, we discuss possible generation mechanisms for postmidnight FAIs.

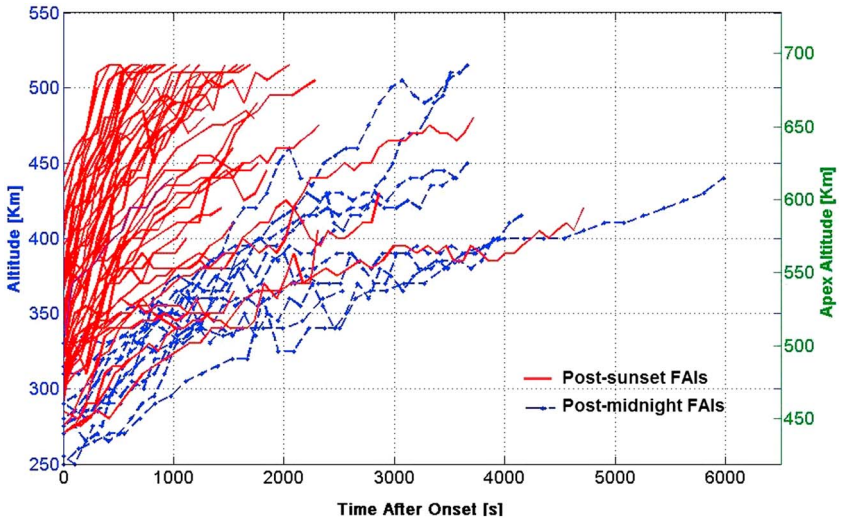

Figure 2. Temporal variation of the top altitude of the FAIs observed with the EAR during the growth phase. The left vertical axis shows the altitude of the location where the EAR radar beam is perpendicular to the magnetic field line. The right vertical axis shows the apex altitude of the geomagnetic field line connecting to the point measured with the EAR.

2. Observations and Results

The EAR is located at Kototabang (0.2°S, 100.3°E; 10.4°S geomagnetic latitude). It is a large monostatic radar that operates at 47.0 MHz with a peak output power of 100 kW. By allocating the radar beam in the direction perpendicular to the geomagnetic field, 3 m scale FAIs in the ionosphere can be observed [*Fukao et al*., 2003]. Using an active phased array antenna system, the EAR can steer the radar beam rapidly on a pulse-to-pulse basis. We conducted 16 beam measurements for the *F* region FAI. This mode allowed us to plot the FAI echo intensity for a fan-shaped range azimuth sector (fan sector) map that covers 600 km in the zonal direction (~5° in longitude) at an altitude of 450 km and in the altitude range of 168–515 km [*Fukao et al*., 2004; *Yokoyama and Fukao*, 2006]. The fan sector map is obtained at ~2 min intervals. Using this map of the FAI echo intensity, we can investigate the spatiotemporal variations of the FAIs independently and thus distinguish between developing FAIs and FAIs drifting into the radar's FOV [e.g., *Ajith et al*., 2015]. In the present paper, we have analyzed FAI data obtained with the EAR from May 2010 to June 2013 and studied events of the evolving FAIs. We selected events in which the FAIs with the signal-to-noise ratio larger than 0 dB continued more than 10 min. Considering previous studies of seasonal and local time variations of FAI occurrence [*Otsuka et al*., 2009, 2012; *Nishioka et al*., 2012], in this study, we refer to the evolving FAIs appearing between 19:00 and 21:00 LT as postsunset and those appearing after 22:30 LT as postmidnight FAIs. Developing FAIs were not observed between 21:00 and 22:30 LT at EAR. During this local time, only FAIs drifting into the FOV were observed.

Figure 1 shows a time sequence of the fan sector maps of the FAI echo intensity as observed with the EAR between 00:09 and 01:15 LT on 24 July 24 2012. This is a typical example showing the onset and development of postmidnight FAIs in the fan sector map. A small echo region appears at 00:16 LT at an altitude of ~270 km, and it successively grows to higher altitudes; furthermore, its echo intensity increases for an hour. This FAI region reaches the top of the radar's FOV at 01:15 LT. To estimate the vertical rise velocity of the FAI structure, the top altitude of the FAI echo with signal-to-noise ratio exceeding −3 dB is determined within each fan sector map during its growth phase until the FAI reaches the maximum altitude of the FOV, stops extending in altitude, or drifts out of the radar FOV. The top altitudes are obtained at a 2 min interval.

Figure 2 shows the temporal evolution of the top altitudes of 15 postmidnight and 50 postsunset FAI events during their growth phases. The left vertical axis shows the altitude of the location where the EAR radar beam is perpendicular to the magnetic field line. The right axis shows the apex altitude of the geomagnetic field line connecting to the point measured with the EAR. We used the International Geomagnetic Reference

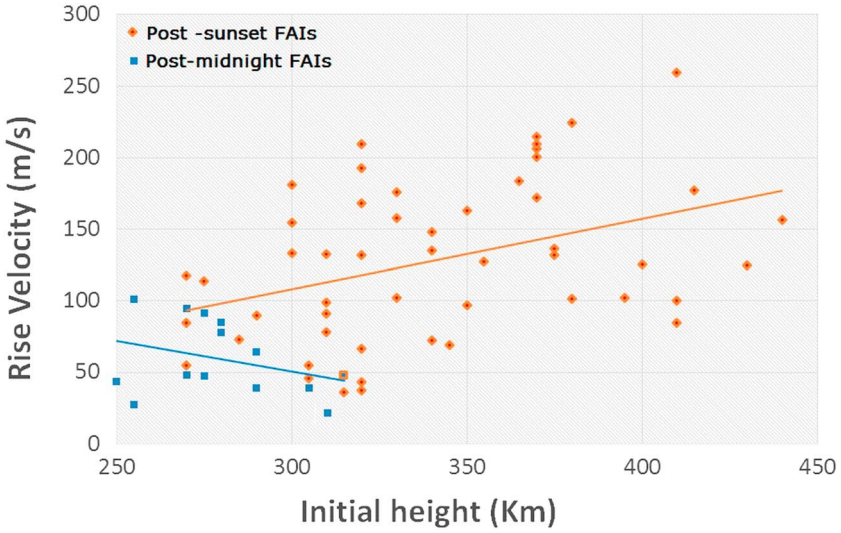

Figure 3. Relationship of rise velocity of the FAI and initial altitude at which FAIs are observed with the EAR. Red and blue symbols represent postsunset and postmidnight FAIs, respectively. Solid lines indicate the regression lines for postsunset and postmidnight FAIs.

Field (IGRF) model [*Thébault et al*., 2015] to calculate the apex altitude. The horizontal axis shows the time in seconds from the first detection of FAI by the EAR. This figure shows that most postsunset FAIs (red curves) start at altitudes higher than 320 km. They extend rapidly to higher altitudes and quickly reach the maximum detectable altitude of the EAR (~515 km) within a short period of ~2000 s from the onset, although a few post-sunset FAIs rise slowly and are confined to altitudes of less than 500 km. In contrast, the initial top altitudes of postmidnight FAIs (blue dashed curves) are mostly seen below 320 km. Because the growth in altitude of the postmidnight FAIs is slower than postsunset ones, the growth of the postmidnight FAIs sometimes can be observed for more than 1 h, and most of them do not exceed an altitude of 450 km. Slope of each curve in Figure 2 represents rise velocity of the FAI. As seen in the figure, the rise velocities tend to decrease with time as the bubble grows. Therefore, we calculated the rise velocity for each FAI event from the top altitudes of the FAIs observed for the first 15 min interval by using the least squares method.

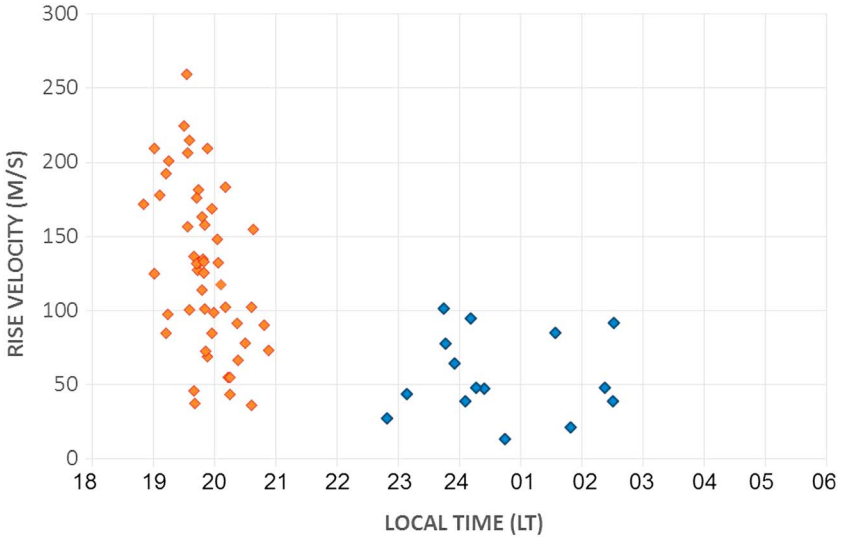

Figure 4. Local time variation of the rise velocity of postsunset (red triangles) and postmidnight (blue diamonds) FAIs observed with the EAR.

In Figure 3, the rise velocities of the postsunset (red diamonds) and postmidnight (blue squares) FAIs during their growth phase are plotted as a function of the initial altitude of the FAIs. The initial altitudes of the postmidnight FAIs are mostly below 320 km, whereas those of the postsunset FAIs exhibit a larger variability, from 270 to 440 km. We found that the rise velocities of postsunset FAIs tend to increase linearly with their initial altitudes. We expect, in general, that the stronger the PRE that lifts the ionosphere postsunset, the stronger the Rayleigh-Taylor growth rate is and the stronger the polarization electric fields that create the rise velocity of the bubble and the embedded FAI will be. In contrast, the initial altitude and rise velocity for postmidnight FAIs show no clear correlation or perhaps a negative correlation.

Figure 4 shows the local time variation of FAI rise velocities for 15 postmidnight and 50 postsunset FAI events. The rise velocities of postmidnight FAIs vary between 10 and 100 m/s, whereas postsunset FAIs show a larger variability between 35 and 260 m/s. The rise velocities of postsunset FAIs decrease rapidly with local time from 19:30 to 21:00 LT. The postsunset FAIs mostly appear for 2 h, from 19:00 to 21:00 LT, whereas the appearance of postmidnight FAIs is widely distributed between 22:30 and 02:30 LT. Developing FAIs were not observed between 21:00 and 22:30 LT although several FAIs drifting from either eastern or western side of the EAR's FOV were detected in this period.

3. Discussion

Two mechanisms have been proposed for the generation of postmidnight FAIs. The first possibility is that FAIs are associated with MSTIDs [e.g., *Otsuka et al*., 2009]. At midlatitudes, FAIs coexist with MSTIDs, which tend to propagate to lower latitudes. The second possibility is that FAIs exist within plasma bubbles that have developed as a consequence of the Rayleigh-Taylor or other instability. In this paper, we study FAIs which have appeared and grown upward within the FOV of the EAR and thus consider only the second mechanism.

Since Kototabang is located approximately 10° south of the magnetic equator, there are two possibilities for the time when a plasma bubble is generated and observed as postmidnight FAI by the EAR. One is that plasma bubble is generated at the sunset terminator, growing very slowly upward and reaching at Kototabang around midnight [*Abdu*, 2012]. The other is plasma bubble generated closer to midnight but rises faster. In order to distinguish between these two possibilities, we have estimated the earliest local time when the plasma bubbles could have been initiated at the magnetic equator. Using the IGRF model, we calculated the apex altitude (h_a (km)) of the magnetic field line connecting to the region where the postmidnight FAIs were initially observed using the EAR. The rise velocity of the postmidnight FAI (plasma bubble) over the equator (v_a (m/s)) is calculated from the rise velocity of the observed FAIs along the radar beam, supposing that plasma bubbles are elongated along the magnetic field line. We also assumed that the plasma bubble is initiated at an altitude of 250 km at the magnetic equator and that it grows to higher altitudes at a constant rise velocity (v_a). The interval of the plasma bubble growth from its initial altitude (250 km) to h_a is obtained by the following formula $t = \frac{(h_a - 250) \times 1000}{v_a}$ (s). We calculated the period for each postmidnight event and estimated the local time when the plasma bubble is initiated at the magnetic equator (Table 1). We found that plasma bubble initiation could occur between 21:37 and 01:56 LT for all the postmidnight FAIs, except for the event on 19 May 2010. Therefore, these results could suggest that most postmidnight FAIs observed with the EAR are accompanied by plasma bubbles initiated well after the PRE ceases.

The rise velocities of the postsunset FAIs observed in 50 cases were found to vary between 25 and 260 m/s. By using the EAR, *Yokoyama and Fukao* [2006] calculated the rise velocity of 11 upwelling FAIs in the growth phase at postsunset between October 2002 and April 2004 during moderate solar activity and found that the velocities range from 45 to 261 m/s. At other sites, by using two-dimensional maps of FAIs observed with the Advanced Research Project Agency (ARPA) Long-range Tracking and Identification Radar, *Tsunoda* [1981] reported that FAIs develop upward with rise velocities ranging from 125 to 350 m/s. *Dabas and Reddy* [1990] determined the rise velocities of plasma bubbles based on scintillation observations. They found that the velocities range from 128 to 416 m/s at altitudes of 450–550 km and that they decrease with increasing altitude above 550 km. Compared to these previous studies, the rise velocities obtained in this study tend to be smaller, probably because they have been obtained under low solar activity conditions. The eastward electric fields at the magnetic equator at the sunset terminator play an important role in generating plasma bubbles through the Rayleigh-Taylor instability. Here we consider the linear growth rate of the Rayleigh-

Table 1. List of Evolving Postmidnight FAIs Observed With EAR

Date	Initial Time at EAR (LT)	Initial Altitude at EAR (km)	Apex Altitude at ME[a] (km)	Rise Velocity at ME[a] (m/s)	Estimated Initiated Time at ME[a] (LT)
19 May 2010	0:44	330	501	13	*19:33*
9 July 2010	23:08	250	419	44	22:05
13 July 2010	1:49	310	480	21	22:56
15 July 2010	0:05	305	475	39	22:31
31 July 2010	0:24	275	445	47	23:15
15 May 2011	0:11	270	440	95	23:38
10 June 2011	1:34	280	450	85	0:55
26 June 2011	23:44	255	424	99	23:16
4 July 2011	23:55	290	460	64	23:02
4 June 2012	2:22	315	485	48	1:03
6 June 2012	23:46	280	450	78	23:04
5 July 2012	22:49	255	424	40	21:37
24 July 2012	0:16	270	440	65	23:11
11 June 2013	2:31	275	445	92	1:56
26 June 2013	2:30	290	460	39	1:01

[a]ME: magnetic equator.

Taylor instability (γ), which can be described as $\gamma = \left(\frac{E}{B} + \frac{g}{\nu_{in}}\right)\frac{1}{N}\frac{\partial N}{\partial z}$, where E, B, g, N, ν_{in}, and z are the eastward electric field, magnetic field, gravity acceleration, plasma density, ion-neutral collision frequency, and altitude, respectively. When E is eastward and large, the growth rate becomes large. E is enhanced by PRE at the sunset terminator and becomes larger during high solar activity than during low solar activity. A weaker PRE at solar minimum also reduces the lift of the F layer postsunset and thus reduces the magnitude of the g/ν_{in} term, further weakening the Rayleigh-Taylor growth rate. The growth rate is an indicator of the magnitude of the polarization electric fields which will later cause the rise of the bubbles in the nonlinear phase of their development, so solar minimum should also mean lower bubble rise velocities. Thus, this solar activity dependence of E could be responsible for the low rise velocities observed here compared to those reported in other papers.

During nighttime, E is generally westward [*Fejer et al*., 1991], which can make the Rayleigh-Taylor growth rate small or negative. By analyzing the ionosonde data obtained near magnetic equator in Thailand, *Nishioka et al*. [2012] have reported that the F layer is high after midnight at around June solstice under low solar activity conditions and shown that the increase in g/ν_{in} due to the uplift of the F layer can compensate for the prevailing westward electric fields in the postmidnight local time, making the growth rate positive.

Using Communication/Navigation Outage Forecasting System (C/NOFS), recently, *Stoneback et al*. [2011] showed that the vertical drift near midnight was sometimes positive in the Northern Hemisphere (60°–120° longitude sector, which includes EAR site) in 2009. This result indicates a possibility of eastward zonal electric field that lifts the F layer up and enhances the growth rate of the Rayleigh-Taylor instability around midnight under low solar activity conditions. However, the mean vertical ion drift in this sector overall was still downward in 2010 [*Stoneback et al*., 2011], whereas the postmidnight FAIs were observed with the EAR; it remains to be seen if the frequency of upward postmidnight drifts matches the occurrence of observation of postmidnight FAIs with the EAR in 2010. Also, *Stoneback and Heelis* [2014] pointed out that longitudinal variation of occurrence in the irregularities of the plasma density and ion drift velocity observed in C/NOFS satellite is not consistent with that of the vertical ion drift.

Nicolls et al. [2006] have showed that the postmidnight uplifts near the magnetic equator occur fairly regularly. They showed that upward shifts in the height of the F layer need not be caused by eastward electric fields but can be produced by a combination of decreasing westward electric field with sufficient recombination process which eats away at the bottom of the F layer. This zonal electric field is daily produced by the dynamo action of the thermospheric winds, augmented by fields impressed, or induced by geomagnetic activity. A decreasing westward electric field could be caused by a change in the wind system related to the midnight temperature maximum (MTM). MTM is considered to be caused by convergence of the thermospheric neutral winds around midnight. Once the MTM, corresponding to the pressure bulge around

midnight, is formed, abatement of the equatorward winds can occur due to the pressure gradient forces and result in weakening westward electric field through the *F* region dynamo. *Maruyama et al*. [2008], who have derived meridional neutral winds from magnetically conjugate observations of ionosondes at low latitudes, have reported that the expected abatement of the equatorward winds is not seen. MTM is driven by tidal waves; in particular, the terdiurnal tide propagates upward from the lower atmosphere [*Akmaev et al*., 2010]. The day-to-day variability of the tides may also be responsible for the wide distribution of the local time when the postmidnight FAIs occur. Further studies will be needed to reveal wind system associated with the MTM and how they affect the electric fields produced by dynamo action.

Our observations show that most postmidnight plasma bubbles do not exceed an altitude of 450 km, whereas plasma bubbles at postsunset mostly exceed the maximum range of the EAR measurement (~515 km). This result suggests that the polarization electric fields within the plasma bubbles are smaller at postmidnight than at postsunset. The FAI observed by the 47 MHz EAR is plasma density perturbations with scale size of approximately 3 m. Such meter-scale irregularities are considered to be generated by plasma instabilities, in which electric fields play an important role. Especially, the FAIs within plasma bubbles could be caused by the coupling processes between the lower hybrid drift and the low-frequency drift instabilities [*Ossakow*, 1981]. The large electric fields could induce more active instability and probably cause intense FAI echo. Conversely, weak polarization electric fields, along with lower plasma densities, at postmidnight could reduce the echo intensity of the FAIs. In fact, based on the 30.8 MHz radar measurements of the FAIs in Indonesia, *Otsuka et al*. [2009] reported that the echo intensity of the FAIs is weaker at postmidnight than at postsunset.

Figure 3 shows a positive correlation between the initial altitude and the rise velocity for the postsunset FAIs but a small range of initial altitudes and small or negative correlation between the initial altitude and the rise velocity for postmidnight FAIs. This could indicate the difference in the mechanism producing the instability in these two cases: If the rise of the *F* layer that produces the instability in the postmidnight case is due to recombination with minimal electric field, then the variability of the initial altitude would be reduced because the variability of the neutral densities that drive recombination is much smaller than the variability of the electric fields which drive the uplift of the *F* layer in the postsunset case.

4. Summary

We have analyzed the *F* region FAIs observed in a mode of 16 beam measurements with the EAR at Kototabang, Indonesia, from May 2010 to June 2013 to study the growth phase of the FAIs using fan sector maps of the FAI echoes. The observed features of the postsunset and postmidnight FAIs can be summarized as follows:

1. The rise velocities of the postmidnight FAIs are between 10 and 100 m/s and smaller than those at postsunset FAIs (from 35 to 260 m/s).
2. Most of the postmidnight FAIs do not exceed an altitude of 450 km.
3. The postmidnight FAIs were observed in a wide range of local times, between 22:30 and 02:30 LT, whereas the postsunset FAIs appeared in a narrower range, from 19:00 to 21:00 LT.
4. The earliest conceivable time for the creation of the postmidnight FAIs is 21:30 LT, well after the interval of postsunset Rayleigh-Taylor instability.
5. Although the postsunset FAIs show a large range of initial altitudes and a clear positive correlation between their initial altitudes and rise velocities, the postmidnight FAIs form in a small range of initial altitudes and do not show such a clear correlation.

From these results, we conclude that most postmidnight FAIs observed with the EAR are accompanied by plasma bubbles generated at the magnetic equator after the PRE ceases. The growth rate of the Rayleigh-Taylor instability is smaller at postmidnight than at postsunset, and weaker polarization fields result in slower rise velocities. The shift in the height of the *F* layer that produces the instability could be caused by bottom-side recombination accompanied by either eastward electric fields or weakened westward electric fields, which may be produced by the tidal winds that cause the MTM. If so, then the day-to-day variability of the tides producing MTM may be responsible for the wide distribution of the local time when the postmidnight FAIs occur.

Acknowledgments
The EAR is operated by the Research Institute for Sustainable Humanosphere (RISH), Kyoto University, and the Indonesian National Institute of Aeronautics and Space (LAPAN). This work was supported by Grants-in-Aid for Scientific Research (25302007, 15H02135, and 15H05815) from the Japan Society for the Promotion of Science and by the Leadership Development Program for Space Exploration and Research, Nagoya University. We also had the support of the Inter-university Upper atmosphere Global Observation NETwork (IUGONET) of the Ministry of Education, Culture, Sports, Science and Technology (MEXT), Japan, and the International Joint Research Program of STEL, Nagoya University. The work of S. Tulasi Ram is supported by STEL international joint research program.

References

Abdu, M. A. (2012), Equatorial spread F development and quiet time variability under solar minimum condition, *Indian J. Radio Space Phys.*, *41*, 168–183.

Ajith, K. K., S. T. Ram, M. Yamamoto, T. Yokoyama, V. S. Gowtam, Y. Otsuka, T. Tsugawa, and K. Niranjan (2015), Explicit characteristics of evolutionary-type plasma bubbles observed from Equatorial Atmosphere Radar during the low to moderate solar activity years 2010–2012, *J. Geophys. Res. Space Physics*, *120*, 1371–1382, doi:10.1002/2014JA020878.

Akmaev, R. A., F. Wu, T. J. Fuller-Rowell, H. Wang, and M. D. Iredell (2010), Midnight density and temperature maxima, and thermospheric dynamics in Whole Atmosphere Model simulations, *J. Geophys. Res.*, *115*, A08326, doi:10.1029/2010JA015651.

Burke, W. J., L. C. Gentile, C. Y. Huang, C. E. Valladares, and S. Y. Su (2004), Longitudinal variability of equatorial plasma bubbles observed by DMSP and ROCSAT-1, *J. Geophys. Res.*, *109*, A12301, doi:10.1029/2004JA010583.

Candido, C. M. N., I. S. Batista, F. Becker-Guedes, M. A. Abdu, J. H. A. Sobral, and H. Takahashi (2011), Spread F occurrence over a southern anomaly crest location in Brazil during June solstice of solar minimum activity, *J. Geophys. Res.*, *116*, A06316, doi:10.1029/2010JA016374.

Dabas, R. S., and B. M. Reddy (1990), Equatorial plasma bubble rise velocities in the Indian sector determined from multistation scintillation observations, *Radio Sci.*, *25*, 125–132, doi:10.1029/RS025i002p00125.

Fejer, B. G., E. R. de Paula, S. A. Gonzalez, and R. F. Woodman (1991), Average vertical and zonal F region plasma drifts over Jicamarca, *J. Geophys. Res.*, *96*(A8), 13,901–13,906, doi:10.1029/91JA01171.

Fukao, S., H. Hashiguchi, M. Yamamoto, T. Tsuda, T. Nakamura, M. K. Yamamoto, T. Sato, M. Hagio, and Y. Yabugaki (2003), Equatorial Atmosphere Radar (EAR): System description and first results, *Radio Sci.*, *38*(3), 1053, doi:10.1029/2002RS002767.

Fukao, S., Y. Ozawa, T. Yokoyama, M. Yamamoto, and R. T. Tsunoda (2004), First observations of the spatial structure of *F* region 3-m-scale field-aligned irregularities with the Equatorial Atmosphere Radar in Indonesia, *J. Geophys. Res.*, *109*, A02304, doi:10.1029/2003JA010096.

Haerendel, G. (1974), *Theory of Equatorial Spread F, Preprint*, Max Planck Inst. Extraterr. Phys., Munich, Germany.

Heelis, R. A., R. Stoneback, G. D. Earle, R. A. Haaser, and M. A. Abdu (2010), Medium-scale equatorial plasma irregularities observed by Coupled Ion-Neutral Dynamics Investigation sensors aboard the Communication Navigation Outage Forecast System in a prolonged solar minimum, *J. Geophys. Res.*, *115*, A10321, doi:10.1029/2010JA015596.

Kelley, M. C. (2009), *The Earth's Ionosphere: Plasma Physics and Electrodynamics*, 2nd ed., Academic, Burlington, Mass.

Maruyama, T., S. Saito, M. Kawamura, and K. Nozaki (2008), Thermospheric meridional winds as deduced from ionosonde chain at low and equatorial latitudes and their connection with midnight temperature maximum, *J. Geophys. Res.*, *113*, A09316, doi:10.1029/2008JA013031.

Miller, E. S., J. J. Makela, K. M. Groves, M. C. Kelley, and R. T. Tsunoda (2010), Coordinated study of coherent radar backscatter and optical airglow depletions in the central Pacific, *J. Geophys. Res.*, *115*, A06307, doi:10.1029/2009JA014946.

Nicolls, M. J., M. C. Kelley, M. N. Vlasov, Y. Sahai, J. L. Chau, D. L. Hysell, P. R. Fagundes, F. Becker-Guedes, and W. L. C. Lima (2006), Observations and modeling of post-midnight uplifts near the magnetic equator, *Ann. Geophys.*, *24*, 1317–1331, doi:10.5194/angeo-24-1317-2006.

Nishioka, M., Y. Otsuka, K. Shiokawa, T. Tsugawa, Effendy, P. Supnithi, T. Nagatsuma, and K. T. Murata (2012), On post-midnight field-aligned irregularities observed with a 30.8-MHz radar at a low latitude: Comparison with *F*-layer altitude near the geomagnetic equator, *J. Geophys. Res.*, *117*, A08337, doi:10.1029/2012JA017692.

Ossakow, S. L. (1981), Spread-F theories—A review, *J. Atmos. Terr. Phys.*, *43*, 437–452.

Otsuka, Y., T. Ogawa, and Effendy (2009), VHF radar observations of nighttime F-region field-aligned irregularities over Kototabang, Indonesia, *Earth Planets Space*, *61*(4), 431–437.

Otsuka, Y., K. Shiokawa, M. Nishioka, and Effedy (2012), VHF Radar Observations of Post-Midnight F-Region Field-Aligned Irregularities over Indonesia during Solar Minimum, *Indian J. Radio Space Phys.*, *41*, 199–207.

Patra, A. K., D. V. Phanikumar, and T. K. Pant (2009), Gadanki radar observations of *F* region field-aligned irregularities during June solstice of solar minimum: First results and preliminary analysis, *J. Geophys. Res.*, *114*, A12305, doi:10.1029/2009JA014437.

Stoneback, R. A., and R. A. Heelis (2014), Identifying equatorial ionospheric irregularities using in situ ion drifts, *Ann. Geophys.*, *32*, 421–429, doi:10.5194/angeo-32-421-2014.

Stoneback, R. A., R. A. Heelis, A. G. Burrell, W. R. Coley, B. G. Fejer, and E. Pacheco (2011), Observations of quiet time vertical ion drift in the equatorial ionosphere during the solar minimum period of 2009, *J. Geophys. Res.*, *116*, A12327, doi:10.1029/2011JA016712.

Thébault, E., et al. (2015), International geomagnetic reference field: The 12th generation, *Earth Planets Space*, *67*, 79, doi:10.1186/s40623-015-0228-9.

Tsunoda, R. T. (1981), Time evolution and dynamics of equatorial backscatter plumes. 1. Growth phase, *J. Geophys. Res.*, *86*(A1), 139–149, doi:10.1029/JA086iA01p00139.

Tsunoda, R. T. (1985), Control of the seasonal and longitudinal occurrence of equatorial scintillations by the longitudinal gradient in integrated *E* region Pedersen conductivity, *J. Geophys. Res.*, *90*, 447–456, doi:10.1029/JA090iA01p00447.

Woodman, R. F., and C. LaHoz (1976), Radar observations of *F* region equatorial irregularities, *J. Geophys. Res.*, *81*, 5447–5466, doi:10.1029/JA081i031p05447.

Yokoyama, T., and S. Fukao (2006), Upwelling backscatter plumes in growth phase of equatorial spread *F* observed with the Equatorial Atmosphere Radar, *Geophys. Res. Lett.*, *33*, L08104, doi:10.1029/2006GL025680.

Yokoyama, T., S. Fukao, and M. Yamamoto (2004), Relationship of the onset of equatorial *F* region irregularities with the sunset terminator observed with the Equatorial Atmosphere Radar, *Geophys. Res. Lett.*, *31*, L24804, doi:10.1029/2004GL021529.

Yokoyama, T., R. F. Pfaff, P. A. Roddy, M. Yamamoto, and Y. Otsuka (2011), On postmidnight low-latitude ionospheric irregularities during solar minimum: 2. C/NOFS observations and comparisons with the Equatorial Atmosphere Radar, *J. Geophys. Res.*, *116*, A11326, doi:10.1029/2011JA016798.